Radio wave propagation in the presence of a coastline

Mark D. Casciato, Shadi Oveisgharan, and Kamal Sarabandi

Radiation Laboratory, Department of Electrical Engineering and Computer Science, University of Michigan, Ann Arbor, Michigan, USA

Received 12 April 2002; revised 22 April 2003; accepted 30 June 2003; published 7 October 2003.

[1] In this paper the effect of a coastline on radio wave propagation is analyzed. The coastline consists of a shoreline or land/sea transition in the presence of a cliff or bluff. The problem of diffraction from the transition, when excited by a small dipole, is first addressed. By application of a perturbation technique the effects of a gradual, as opposed to an abrupt transition on the radio wave are discussed. For the case of both source and observation near the surface it is shown that the received fields are independent of the gradient of the transition and that the effects of the land/sea transition on the total fields are dominant, even distant from the transition. This is a very important and counter-intuitive result which has not been reported previously. A UTD solution for an impedance wedge and plane wave excitation is then applied, in order to analyze the combined effect of the land/sea transition and a cliff or bluff on the total received fields. Results are shown for the case of an observation platform (such as an aerial vehicle) flying low over the sea and then up and over the bluff. *INDEX TERMS:* 0669 Electromagnetics: Scattering and diffraction; 0689 Electromagnetics: Wave propagation (4275); 0619 Electromagnetics: Electromagnetic theory; *KEYWORDS:* scattering, diffraction, propagation, electromagnetics, coastal diffraction

Citation: Casciato, M. D., S. Oveisgharan, and K. Sarabandi, Radio wave propagation in the presence of a coastline, *Radio Sci.*, *38*(5), 1085, doi:10.1029/2002RS002696, 2003.

1. Introduction

[2] The simulation of radio wave propagation near the Earth's surface is of practical importance for assessing the performance of wireless systems. In order to create a comprehensive channel model, wave diffraction models for different obstacles and discontinuities must be developed. One scenario to consider is that of a coastline, where a transmitting antenna sits atop or near a cliff or bluff overlooking a shoreline or land/sea transition. The effects of both the cliff and the transition on the radio signal, including their mutual interaction, is modeled in this paper. By application of a perturbation technique, the problem of diffraction from a shoreline or land/sea transition is first addressed, including the effect of a gradual impedance transition as opposed to a more abrupt one on the radio signal. The model will then be extended to include the effects of a nearby cliff or bluff by applying standard Uniform Theory of Diffraction (UTD) techniques.

0048-6604/03/2002RS002696

[3] For the problem of diffraction from a land/sea transition, asymptotic techniques such as the Geometrical Theory of Diffraction (GTD) and its extension the Uniform Theory of Diffraction (UTD) have usually been applied. They are only valid however, for abrupt transitions and do not address the more general problem of a gradual land-sea transition. The problem of coastal diffraction was originally examined by *Clemmow* [1953]; however, he did not consider the case of impedance junctions and was not able to derive closed form expressions for the relevant split functions. *Maliuzhinets* [1958] was the first to consider two impedance junctions as a special case of wedge diffraction, and the simpler dual-integral equation method can also be employed [*Senior and Volakis*, 1995]. *Bazer and Karp* [1962] addressed the problem of plane wave diffraction from shorelines in planar land-sea boundaries, using the Wiener-Hopf technique, while *Wait* [1974], *de Jong* [1975], and *Ott* [1992] addressed the diffraction effects caused by an inhomogeneous surface, using an integral equation technique to solve for an attenuation factor. This solution can be shown to be equivalent to a Physical Optics (PO) solution, and is formulated in terms of integrals which must be solved numerically.

[4] When the actual solution of a problem varies only slightly (is perturbed) from a known exact solution, perturbation theory is a viable approach to solve these general problems. In order to analyze a land/sea transition, an analytic solution is applied, in which a one-dimensional (1-D) impedance variation in an infinite impedance surface is characterized as a perturbation from a homogeneous impedance surface, representing the ground plane. The method provides a solution for calculating the diffraction from a surface impedance transition of arbitrary profile, such as a river, shoreline, or trough, when excited by a small dipole of arbitrary orientation. This technique is an extension of a two-dimensional (2-D) model presented by *Sarabandi* [1990] for a resistive sheet when excited by a plane wave. It was shown by *Sarabandi* [1990] that the method could be extended to that of an impedance sheet simply by replacing the resistivity with the complex impedance divided by a factor of two. The technique was extended to include the case of oblique incidence and dipole excitation by *Sarabandi and Casciato* [1999], and this is the formulation applied here.

[5] In order to solve the perturbation problem, an integral equation is first defined on the impedance surface in the Fourier domain, and from this, recursive expressions for the induced surface current of any order are derived. The resulting expressions are analytic and valid for any general one-dimensional impedance transition for which the Fourier transform exists. The limits of the method are the radius of convergence of the perturbation series, and of course the limit of the first-order impedance boundary condition applied [*Sarabandi and Casciato*, 1999; *Senior and Volakis*, 1995]. Asymptotic techniques are then used to solve the field integrals and the resulting expressions are algebraic to first order in the perturbation series.

[6] When a base station, transmitter, or receiver is located on a cliff or bluff near the seashore, the radio signal interacts with both the cliff and seashore. In addition, and depending on the direction of transmission, the surface currents excited by the incident wave in the transition (or cliff) reradiate and excite additional currents in the cliff (or transition) which in turn reradiate. These higher-order effects can have a significant influence on the received signal. In addition line of sight (LOS) transmission may be blocked and the dominant contributor to the received signal is from the fields diffracted off the cliff edge. In order to include the effects of the cliff in the overall model, standard UTD techniques for diffraction from an impedance wedge are applied. These techniques provide a uniform solution through all shadow and reflection boundaries [*Senior and Volakis*, 1995].

[7] While the analytic solution for the impedance transition is a 3-D solution for that of a small dipole radiating in the presence of a 1-D impedance transition, there are currently no asymptotic solutions for the general case of an obliquely incident wave on an impedance wedge with arbitrary wedge angle. Because of this, and for the purpose of this analysis a 2-D UTD solution for an impedance wedge will be applied, and it will be assumed that the source is distant (including secondary sources) from the transition and cliff so that plane wave excitation is assumed, locally.

[8] In the next section the perturbation technique presented by *Sarabandi and Casciato* [1999] is reviewed, and relevant equations are given. The method is then applied to the problem of diffraction from a land/sea transition. An actual land/sea transition is a gradual transition from the impedance of the water to that of the land, and the effects of varying this transition width are analyzed. It is shown that while the effects of the transition on the total fields is significant for observation distances far from the transition, these effects are independent of the gradient of the transition, when both source and observation are near the impedance surface. Following this a coastline will be analyzed by integrating the combined effects of a land/sea transition in proximity to a cliff. A UTD solution for an impedance wedge will be applied to model the cliff edge. Result are then calculated for the case of an aerial vehicle (helicopter, unmanned aerial vehicle (UAV), etc.) flying from the sea, up and over a cliff.

[9] Note that throughout this paper the time convention $e^{-i\omega t}$ is assumed and suppressed. Also the term "scattered fields" implies that all electric field components except the direct are included, while "diffracted fields" does not include either the direct or reflected (Geometrical Optics (GO)) field components.

2. Land/Sea Transition

[10] This section begins by presenting a brief review of the perturbation technique. The case of plane wave excitation is first discussed, followed by the extension of the method to small dipole excitation. Its application to a land/sea transition follows, including analysis and results. Interested readers are again referred to *Sarabandi and Casciato* [1999] for a detailed discussion of the technique.

2.1. Review of the Perturbation Method: Plane Wave Excitation

[11] The geometry of the problem is as shown in Figure 1 with θ and ϕ as defined in standard spherical coordinates. Noting that the geometry is uniform in y and thus the propagation constant of the scattered field must match that of the incidence field along the y dimension, the scattered field can only exist along the specular cone,

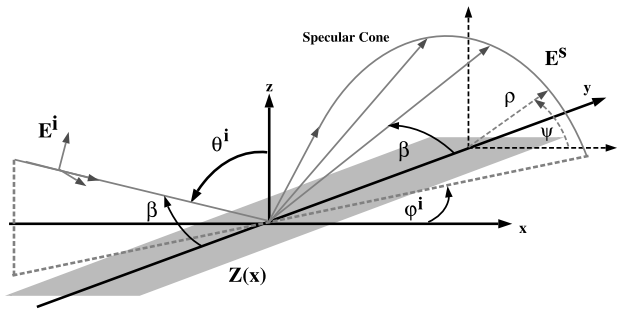

Figure 1. Scattering geometry for variable impedance surface. See color version of this figure in the HTML.

as is seen in Figure 1. The assumption made is that of a lossy Earth, which is a highly conductive, dielectric medium, and thus the standard impedance boundary condition (SIBC) ($\hat{n} \times \hat{n} \times \mathbf{E}) = -Z(x)(\hat{n} \times \mathbf{H})$) is applied on the surface with **E**, **H** being the electric and magnetic field vectors, respectively, $Z(x)$ the impedance parameter as a function of x, and obviously bold face type indicates a vector quantity. An integral equation for the total tangential electric fields, evaluated on the impedance surface, can be written as

$$\mathbf{E}^T = \left(\mathbf{E}^i + \mathbf{E}^r + \mathbf{E}^d\right)\big|_{z=0} = Z(x)\mathbf{J}(x), \tag{1}$$

where the superscripts T, i, r, and d are indicative of the total, incident, reflected, and diffracted fields, respectively, with **J** denoting the induced surface currents.

[12] To derive the perturbation formulation, the surface impedance $Z(x)$ in equation (1) is defined in terms of an unperturbed impedance Z_1, a perturbation parameter Δ, and an impedance transition function $h(x)$, and is given by

$$Z(x) = Z_1(1 + \Delta h(x)). \tag{2}$$

The unknown surface currents in equation (1) are expanded in powers of Δ and a transformation then made into the Fourier domain for ease of analysis. After extensive algebra, recursive expressions are obtained relating successive orders of currents in the perturbation series. The x and y components of the zeroth-order currents (Δ^n, $n = 0$) correspond to the effects of the homogeneous surface of impedance Z_1 (currents which generate GO fields for plane wave incidence), and are given in the Fourier domain as

$$\tilde{J}_{0x}(\alpha) = \frac{\left\{E_{0x}\left[\frac{1}{2}Z_1 + \frac{k_0 Z_0}{2k_z}\sin^2\beta\right] + E_{0y}\left[\frac{Z_0\alpha}{2k_z}\cos\beta\right]\right\}2\pi\delta\left(\alpha - k_x^i\right)}{\left[\frac{1}{2}Z_1 + \frac{k_0 Z_0}{2k_z}\left(1 - \frac{\alpha^2}{k_0^2}\right)\right]\left[\frac{1}{2}Z_1 + \frac{k_0 Z_0}{2k_z}\sin^2\beta\right] - \left(\frac{Z_0\alpha\cos\beta}{2k_z}\right)^2}, \tag{3}$$

$$\tilde{J}_{0y}(\alpha) = \frac{\left\{E_{0y}\left[\frac{1}{2}Z_1 + \frac{k_0 Z_0}{2k_z}\left(1 - \frac{\alpha^2}{k_0^2}\right)\right] + E_{0x}\left[\frac{Z_0\alpha}{2k_z}\cos\beta\right]\right\}2\pi\delta\left(\alpha - k_x^i\right)}{\left[\frac{1}{2}Z_1 + \frac{k_0 Z_0}{2k_z}\left(1 - \frac{\alpha^2}{k_0^2}\right)\right]\left[\frac{1}{2}Z_1 + \frac{k_0 Z_0}{2k_z}\sin^2\beta\right] - \left(\frac{Z_0\alpha\cos\beta}{2k_z}\right)^2}. \tag{4}$$

In equations (3) and (4), α is the Fourier domain variable, E_{0x} and E_{0y} the components of the excitation field, and k_0 and Z_0 the free space propagation constant and characteristic impedance, respectively. Also k_z is the dependent variable in the field integrals, given by $k_z = \sqrt{\alpha - k_0^2}$, k_x^i is the x component of the incident field propagation constant, and $\hat{k}^i \cdot \hat{y} = \cos\beta = \sin\theta^i \sin\phi^i$.

[13] Higher-order terms for the unknown surface currents in the Fourier domain are given by the following recursive expressions:

$$\tilde{J}_{(n+1)x}(\alpha) = \frac{1}{2\pi}\left[\frac{\left(\frac{k_z\eta}{k_0}\right)\left[\left(\frac{k_z\eta}{k_0}\right) + \sin^2\beta\right]\tilde{h}(\alpha)*\tilde{J}_{nx}(\alpha) + \frac{k_z\eta}{k_0}\frac{\alpha}{k_0}\cos\beta\tilde{h}(\alpha)*\tilde{J}_{ny}(\alpha)}{\left(1 + \frac{k_z\eta}{k_0}\right)\left\{\frac{\alpha^2}{k_0^2} - \sin^2\beta - \frac{k_z\eta}{k_0}\right\}}\right], \tag{5}$$

$$\tilde{J}_{(n+1)y}(\alpha) = \frac{1}{2\pi}\left[\frac{\left(\frac{k_z\eta}{k_0}\right)\left[\left(\frac{k_z\eta}{k_0}\right) + \left(1 - \frac{\alpha^2}{k_0^2}\right)\right]\tilde{h}(\alpha)*\tilde{J}_{ny}(\alpha) + \frac{k_z\eta}{k_0}\frac{\alpha}{k_0}\cos\beta\tilde{h}(\alpha)*\tilde{J}_{nx}(\alpha)}{\left(1 + \frac{k_z\eta}{k_0}\right)\left\{\frac{\alpha^2}{k_0^2} - \sin^2\beta - \frac{k_z\eta}{k_0}\right\}}\right], \tag{6}$$

where η is the normalized surface impedance given by $\eta = Z_1/Z_0$ and the symbol * in equation (5) and (6) denotes the convolution operator.

[14] Once the induced surface currents are obtained, the diffracted field, for any order current in the perturbation series, can be calculated by application of the radiation integrals. For large observation distances, stationary phase techniques are used to evaluate these integrals, resulting in the following analytic expressions for the far-zone diffracted electric fields generated by surface current of order n, and for plane wave excitation.

$$\mathbf{E}_n^s(\mathbf{r}) = -\frac{k_0 Z_0 \Delta^n}{\sqrt{2\pi k_\rho^i \rho}}\left\{\hat{h}\hat{h} + \hat{v}\hat{v}\right\}\cdot\tilde{\mathbf{J}}_n\left(k_\rho^i\cos\psi\right)e^{i\left(k_\rho^i\rho - \frac{\pi}{4}\right)}e^{ik_y^i y}. \tag{7}$$

In equation (7), ψ is the scattering angle defined from the x axis, and positive towards the z axis, in the $x - z$ plane, ρ the radial distance to the observation point in the $x - z$ plane, with $k_\rho^i = k_0 \sin\beta$, all as seen in Figure 1. Also in

equation (7) the unit vectors $\hat{h}$, $\hat{v}$ are evaluated at the stationary points and are given by

$$\hat{h} = \frac{\mathbf{k} \times \hat{z}}{|\mathbf{k} \times \hat{z}|} = \frac{-k_\rho^i \cos\psi \hat{y} + k_y^i \hat{x}}{\sqrt{k_\rho^{i^2} \cos^2\psi + k_y^{i^2}}} = \frac{-k_\rho^i \cos\psi \hat{y} + k_y^i \hat{x}}{\sqrt{k_0^2 \cos^2\psi + k_y^{i^2} \sin^2\psi}}, \quad (8)$$

and

$$\hat{v} = \frac{1}{k_0}\hat{h} \times \mathbf{k} = \frac{-k_\rho^i k_y^i \sin\psi \hat{y} - k_\rho^{i^2} \sin\psi \cos\psi \hat{x} + \left(k_0^2 \cos^2\psi + k_y^{i^2} \sin^2\psi\right)\hat{z}}{k_0\sqrt{k_0^2 \cos^2\psi + k_y^{i^2} \sin^2\psi}}. \quad (9)$$

2.2. Review of the Perturbation Method: Extension to Short Dipole Excitation

[15] To extend the perturbation solution to include excitation by a short dipole the incident dipole fields are represented in the form of a continuous spectrum of plane waves. The methods of the previous section for plane wave excitation can then be applied to each spectral component and the resulting expressions simply integrated over the entire dipole spectrum. Again stationary phase techniques (first-order saddle point) can be applied to evaluate the resulting integrals when both source and observation are distant from the transition.

[16] Consider a short dipole of length l carrying a sinusoidal current of amplitude I_0 and located at $\mathbf{r}_0 = x_0\hat{x} + y_0\hat{y} + z_0\hat{z}$, whose fields are represented in the spectral domain. Again for the situation where distance between source and observation are large compared to wavelength, and also where both are distant from the transition in terms of wavelength, stationary phase for a 2-D integral can applied to find the dominant spectral component of the incident field. This results in the following formulation for the diffracted electric fields generated by an infinitesimal dipole above an inhomogeneous impedance surface.

$$\mathbf{E}_{d_i n}^d(\mathbf{r}) = \mathbf{X}(\mathbf{K}^i)\frac{2\pi i}{C}e^{ik_0 R_S}. \quad (10)$$

In equation (10), $\mathbf{X}(\mathbf{K}^i)$ corresponds to the solution for plane wave incidence found in equation (7), and $\mathbf{K}^i$ is the incident propagation vector of the dominant dipole spectral component at the stationary point, whose components are given by

$$k_x^i = \frac{-x_0(\rho + \rho_0)}{\rho_0 R_S}k_0 \quad (11)$$

$$k_y^i = \frac{(y - y_0)}{R_S}k_0 \quad (12)$$

$$k_z^i = \frac{z_0(\rho + \rho_0)}{\rho_0 R_S}k_0. \quad (13)$$

Also in equation (10), subscript d_i implies dipole excitation, $R_S = \sqrt{(y-y_0)^2 + (\rho + \rho_0)^2}$, f is the exponential function of the field integral given by $f = k_y^i(y - y_0) - k_x^i x_0 + k_z^i z_0 + k_\rho^i \rho$, and C is the 2-D Wronskian of the exponential function, or

$$C = \sqrt{\frac{\partial^2 f}{\partial k_x^{i^2}}\frac{\partial^2 f}{\partial k_y^{i^2}} - \left(\frac{\partial^2 f}{\partial k_x^i \partial k_y^i}\right)^2}. \quad (14)$$

Explicit expressions for (14) are obtained by evaluating the second derivatives of the exponential function at the stationary point and are given by

$$\frac{\partial^2 f}{\partial k_x^{i^2}} = -\frac{\rho_0^2}{z_0 k_z^i}, \quad (15)$$

$$\frac{\partial^2 f}{\partial k_y^{i^2}} = -\frac{k_z^{i^2} + k_y^{i^2}}{k_z^{i^3}}z_0 - \frac{k_0^2}{\left[k_0^2 - k_y^{i^2}\right]^{3/2}}\rho, \quad (16)$$

$$\frac{\partial^2 f}{\partial k_x^i \partial k_y^i} = -\frac{k_x^i k_y^i}{k_z^{i^3}}z_0. \quad (17)$$

[17] To apply the surface current expressions for plane wave excitation given in equations (5) and (6) to excitation by a small dipole, simply use the appropriate component of the incident dipole electric field for E_{0x} and E_{0y} in equations (5) and (6). The dyadic expression for these incident fields is given by

$$\mathbf{E}_0 = \frac{-I_0 l k_0 Z_0}{8\pi^2}\frac{1}{k_z^i}\left[\hat{l} - \frac{\mathbf{K}^i \cdot \hat{l}\mathbf{K}^i}{k_0^2}\right], \quad (18)$$

where again $\mathbf{K}^i$ is evaluated at the stationary point.

2.3. Application of the Perturbation Method to a Land/Sea Transition

[18] In order to apply the perturbation solution for small dipole excitation to the case of a land/sea transition, we begin with the case of an abrupt transition between land and sea, and then modify the resulting expressions to include the more physical case of a gradual transition. Recall that in the perturbation series,

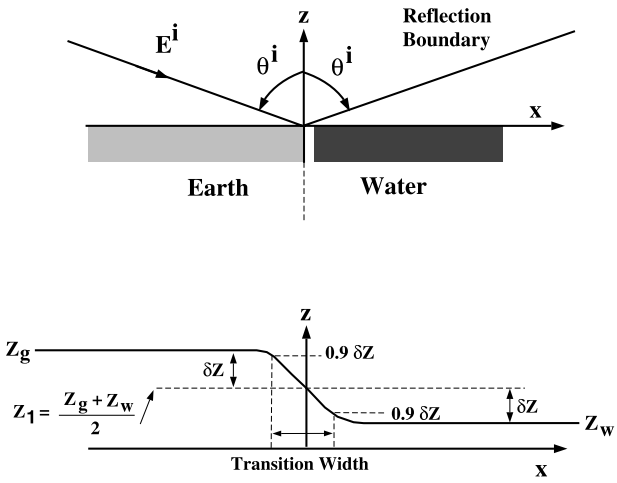

Figure 2. Geometry of a land/sea interface. See color version of this figure in the HTML.

the surface impedance $Z(x)$ given in equation (2) is defined in terms of an unperturbed impedance Z_1 (homogeneous surface), a perturbation parameter Δ, and an impedance transition function, $h(x)$. The impedance transition function for an abrupt land/sea transition can be represented by a unit step function ($h(x) = 0$ for $x < 0$ and $h(x) = 1$ for $x > 0$) with an offset, and this offset is equal to the mean of the land and sea impedances, (Z_1 in Figure 2). For this abrupt transition from one impedance level to another, it is not obvious as to how to represent the unperturbed impedance Z_1, as Z_1 is assumed to be an infinite, homogeneous impedance sheet. In the Fourier domain, where the perturbation technique is applied, the problem becomes more evident. Observing $h(x)$ in the Fourier domain, the Fourier transform of $h(x)$ contains a δ function and the perturbation method cannot be immediately applied. To alleviate this problem, the impedance transition is dealt with in a mean sense, i.e., we assume that the unperturbed impedance, Z_1, is the mean value of the land and sea impedances, or

$$Z_1 = \frac{Z_g + Z_w}{2}, \tag{19}$$

where Z_g and Z_w are the impedances of the land (ground) and sea, respectively, and as seen in Figure 2.

[19] The assumption of a mean impedance as the unperturbed impedance is a valid assumption in terms of the first and higher-order fields in the perturbation series, provided both source and observation are near the impedance surface and distant from each other. This assumption is deduced from the following:

[20] The dipole fields above an impedance half-space can be represented in rigorous form by Sommerfeld integrals [*Sarabandi et al.*, 2002]. These fields correspond to the effects of the homogeneous surface in the perturbation solution for small dipole excitation. (They are represented by the zeroth-order currents in the perturbation series.) These field expressions can be expanded into an asymptotic series, where the lowest-order term in the asymptotic expansion represents the Geometrical Optics (GO) field component which decays as $1/R$, R being the radial distance between source and receiver. For the case considered here (dipole and observation near the impedance surface) this GO component tends to cancel with the direct wave, and higher-order terms in the asymptotic expansion become dominant (Norton surface waves which decay as $1/R^2$; in the literature, see *Norton* [1936, 1937]). The GO component of the fields can be represented as a point image, while the higher-order terms can be interpreted as an extended image source in the complex plane (by application of exact image theory to the Sommerfeld integrals; again see *Sarabandi et al.* [2002]). This extended image represents a smearing in the surface currents and there is no longer a sharp change at the reflection boundary where the GO fields reflected from the land transition to those reflected from the sea. As the reflection boundary is nearer the surface when the source is nearer the surface, the received fields for an observation point distant from the transition and near the surface are a result of this smearing, or mixing of the two surface impedances, and thus the assumption of a mean impedance for the homogeneous surface is valid. As observation and/or source are moved away from the impedance surface the dominant component of the scattered fields becomes the specular (GO) component and the reflection boundary becomes more sharply defined. In this region the mean impedance assumption loses accuracy, however for this case, the space wave (direct + GO) is the dominant contributor to the total fields and the effect of the diffracted fields (those field components generated by the impedance transition) on the total fields can be neglected.

[21] The assumption of a mean impedance allows the impedance transition function to be written directly as a signum function ($sgn(x) = -1/2$ for $x < 0$ and $sgn(x) = 1/2$ for $x > 0$) or

$$h(x) = -sgn(x), \tag{20}$$

whose Fourier transform is given by

$$\tilde{h}(\alpha) = \frac{i}{\alpha}. \tag{21}$$

Applying equation (2), the perturbation parameter Δ is found to be

$$\Delta = \frac{Z_g - Z_w}{Z_1}. \tag{22}$$

[22] In order to represent a more gradual transition function, equation (20) can be modified to

$$h(x) = -sgn(x)\left(1 - e^{-\kappa|x|}\right), \tag{23}$$

which in the Fourier domain becomes

$$\tilde{h}(\alpha) = \frac{i}{\alpha} - \frac{i\alpha}{\alpha^2 + \kappa^2}. \tag{24}$$

In equation (23), κ is a constant parameter, where as $\kappa \rightarrow \infty$ the width of the transition goes to zero, i.e., an abrupt transition.

2.4. Asymptotic Evaluation of Field Integrals for a Land/Sea Transition

[23] In the perturbation series, the first-order diffracted fields (in the far field) from the land/sea transition are proportional to the Fourier transform of the impedance transition function of equation (21). Before beginning analysis of the land/sea transition it is appropriate to note the existence of a simple pole in this impedance transition function, and therefore in the diffracted field integrals. This pole occurs at the reflection boundary of the geometrical optics (GO) fields, and while it can be shown to be a noncontributing pole, care must be taken when evaluating these integrals asymptotically. As the stationary point approaches the pole (observation approaches the reflection boundary) the effect of the stationary point cannot be separated from the effect of the pole and modified asymptotic approaches must be employed. In the literature two approaches are discussed, the additive, and multiplicative method [*Clemmow*, 1950; *Felsen and Marcuvitz*, 1994]. In the additive method the integrand is regularized by subtracting and adding an appropriate factor and the resulting expression expanded in an asymptotic fashion. In the multiplicative method the integrand is regularized, appropriately by a multiplicative factor, and also expanded into an asymptotic series. While both expansions can be shown to be equivalent, the equivalence holds only for the complete asymptotic series of both expansions [*Boersma and Rahmat-Samii*, 1980]. When the series are truncated this equivalence does not hold and the truncated series may produce different results. In the analysis of the land/sea problem only the first-order term in the asymptotic series is retained and it was observed that the multiplicative method produced proper results, while the additive method did not sufficiently compensate for the immediate proximity of the pole, thus implying that higher-order terms in the asymptotic expansion are required to utilize this method.

2.5. Analysis of a Land/Sea Transition

[24] We begin this section by noting that first-order currents only ($\tilde{J}_{1x}, \tilde{J}_{1y}$, $n = 0$ in equations (5) and (6)) are applied throughout this paper in order to generate the diffracted fields from a land/sea transition. Some other relevant factors to mention before beginning analysis are as follows:

[25] 1. As mentioned previously, the standard impedance boundary condition (SIBC) is applied throughout. This approximation is valid through the microwave band. As frequencies increase above the microwave regime, the penetration depth of the impedance surface becomes proportional to wavelength and the accuracy of the SIBC approximation begins to degrade. Note also that results were calculated for a broadband signal from 30 to 130 MHz for the impedance transition and that no dispersive effects were observed in the impulse response of the total fields, for the case of both transmitter and receiver near the impedance surface. Obviously, if either transmitter, receiver, or both, are raised above the impedance surface, the difference in path length between the diffracted/scattered fields, and the direct field will cause a spreading in the impulse response.

[26] 2. At the surface impedances analyzed, surface waves are not a factor. In order to excite a surface wave (this corresponds to capturing a pole in the asymptotic analysis), the surface impedance must be inductive, and the imaginary part of the impedance either equal to or greater than the real part. As the intent of this study is to model a flat, lossy Earth, which is essentially an impenetrable surface, these conditions are not met. As soil moisture is increased and the soil becomes more lossy, the angle of the complex surface impedance in the limit approaches, but does not exceed 45°, so the conditions for excitation of a surface wave are never met.

[27] 3. Many of the results presented are in terms of path loss above free space. Path loss above free space, which will be hereon referred to simply as path loss (PL), is defined as in *Sklar* [1988], where $PL = |E|/|E^i|$, or simply put path loss equals the appropriate received field component, normalized to the magnitude of the incident field.

[28] 4. For all results presented in the next two sections the ground is modeled as San Antonio gray loam, with a density of 1.4 g/cm^3 and gravimetric moisture content of either 10 or 20%. The seawater is approximated by saline water with a salt content of 32.5 *pp*/1000 (a typical value for seawater [*Ulaby et al.*, 1986]). Table 1 presents normalized impedance values for the ground (η_g) and seawater (η_w) for three frequencies analyzed, 30, 150, and 1000 MHz. Also shown in Table 1 is the value of the perturbation parameter Δ for these various frequencies and moisture content.

[29] To begin analysis of the land/sea transition, we first examine the effect of a gradual transition on the diffracted fields. A gradual transition is more representative of an actual land/sea transition, in that physically there can exist no abrupt transition between land and

Table 1. Impedances for Seawater With a 32.5 pp/1000 Salt Content [*Ulaby et al.*, 1986] and Ground Impedances for San Antonio Gray Loam With a Density of 1.4 g/cm^3, for Various Frequencies[a]

Frequency, MHz	η_w	η_g (10% Moisture)	Δ (10% Moisture)	η_g (20% Moisture)	Δ (20% Moisture)
30	0.013 – i0.013	0.15 – i0.09	1.63	0.116 – i0.072	1.54
150	0.03 – i0.03	0.28 – i0.1	1.54	0.213 – i0.056	1.43
1000	0.08 – i0.04	0.37 – i0.04	1.27	0.259 – i0.036	1.03

[a]Values given for the percentage of soil moisture are the gravimetric moisture content of the soil [*Hipp*, 1974].

water in an actual seashore. For this preliminary analysis we examine the case of a vertical electric dipole, operating in the near vicinity of the impedance surface at 30 MHz, and observe the z component of the path loss above free space, of the diffracted electric fields (effects of the impedance transition only). For source and observation near the impedance surface the z components of the scattered field from a vertical electric dipole are the dominant field component for any dipole orientation, and thus is of most interest in the analysis of the transition. The vertical dipole is placed 100λ from the impedance transition, along the negative x axis and 100λ above the impedance surface ($x_0 = -100\lambda$, $y_0 = 0$, $z_0 = 100\lambda$). Observation is across the transition ($y = 0$, restricted to the $x - z$ plane) and at a fixed radial distance of 50λ. The impedance of the ground is representative of San Antonio gray loam with 10% gravimetric moisture content (see Table 1). Figure 3 shows the path loss for transition widths of 0 (abrupt transition), 1, and 10λ, where the transition width is defined as the distance between the points where the transition function is $0.9\delta Z$, where $\delta Z = |Z_g - Z_w|/2$ (see Figure 2). As can be seen in Figure 3, the effect of widening the transition is to focus the diffracted energy in the specular direction ($\psi' = 135°$, where $\psi' = \pi - \psi$). However, in the neighborhood of the specular direction the transition width has little effect on the field levels. This is a significant observation as it indicates that for source and observation near the surface, and again distant from each other and the transition, the width of the transition will have negligible effect on the diffracted fields, as for this scenario the specular angle is pushed to near-grazing observation, i.e., observation is always near the specular point. This makes intuitive sense also as the width of the transition is less apparent as it approaches the horizon of an observer.

[30] To examine further the effects of a land/sea transition on the fields of an infinitesimal dipole, we place a vertical electric dipole at $x_0 = -100\lambda$, $y_0 = 0$, move the source and observation heights to 1, 5, and 10λ (for these examples source and observation are at same height above surface), and compare the path loss of the space wave (direct + GO) to the total fields. The frequency of operation is again at 30 MHz and the observation point is on a straight line parallel to the surface, from $x = -50\lambda$ to $x = 150\lambda$. Note that other parameters are the same as for previous results in this section, with the transition width at zero (abrupt transition). The results are seen in Figures 4a, 4b, and 4c, comparing the space wave to the total fields and showing the results for source/observation heights of 1, 5, and 10λ, respectively.

[31] For this case of source and observation near the impedance surface the Norton surface wave (as noted previously in Section 2.3, higher-order terms in the asymptotic expansion of the field expressions for the homogeneous surface), which decays at a rate of $1/R^2$, is the dominant component of the fields diffracted from the homogeneous surface. Noting that the diffracted fields

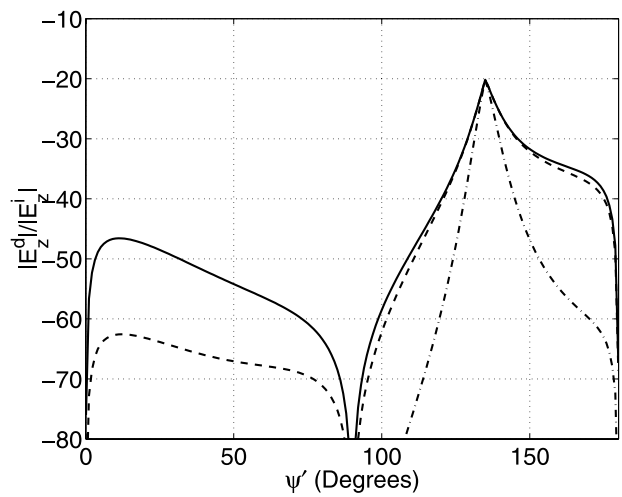

Figure 3. Magnitude (dB) of path loss at 30 MHz, for a land/sea transition located at $x = 0$, z component of the diffracted fields for a vertical (z-directed) electric dipole. Observation ρ is fixed at 50λ, observation $y = 0$, for dipole position of $x_0 = -100\lambda$, $y_0 = 0$, $z_0 = 100\lambda$. Ground moisture is 10%, sea is saline water with a 32.5 *pp*/1000 salt content (see Table 1). Results for transition widths of 0 (solid line), 1 (dashed line), and 10λ (dot-dashed line). See color version of this figure in the HTML.

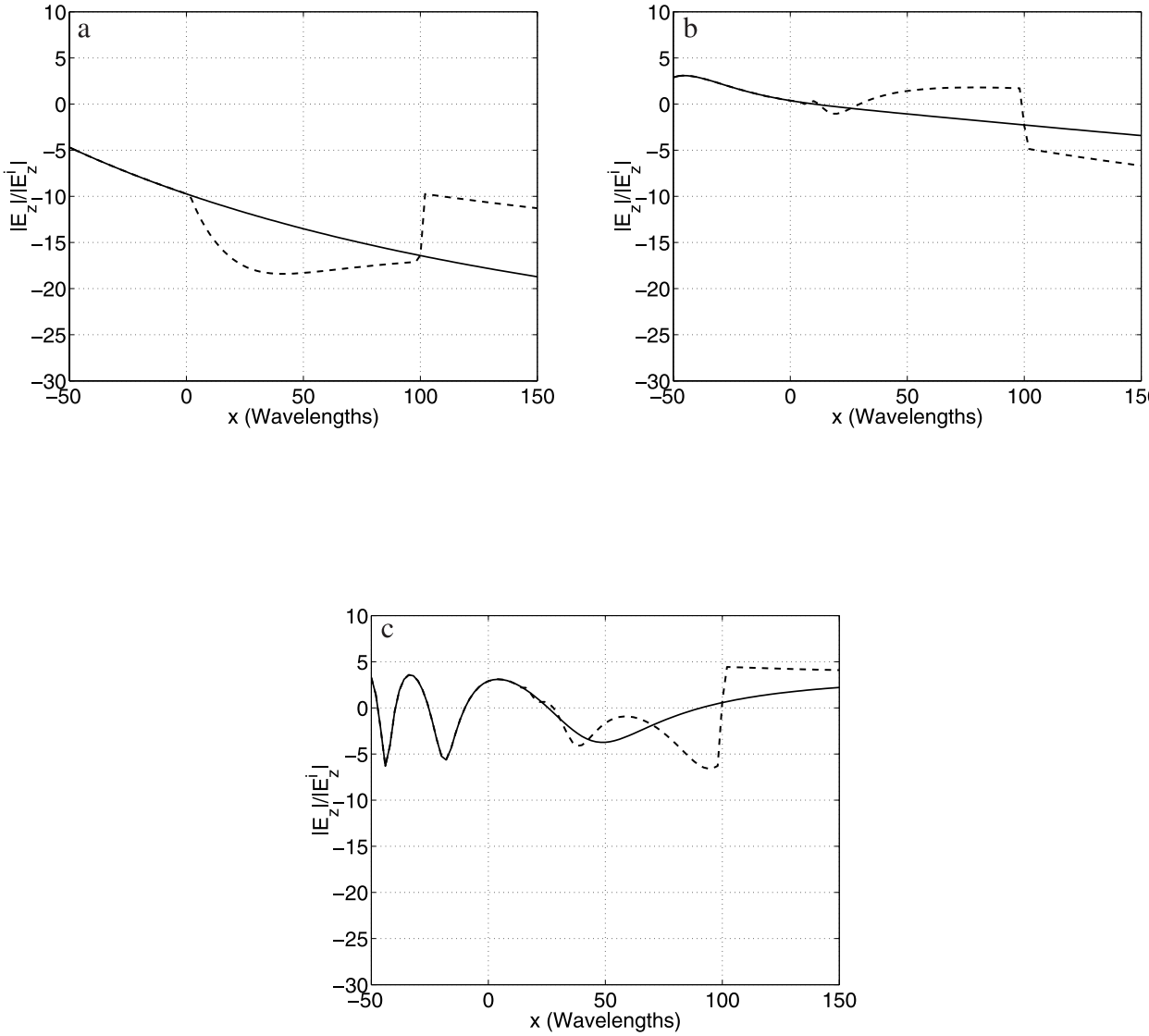

Figure 4. Magnitude (dB) of path loss at 30 MHz, for a land/sea transition, located at $x = 0$, z component of the electric fields for a vertical (z-directed) electric dipole. Transition width is 0λ (abrupt), observation $y = 0$, observation x from -50λ to 150λ. Dipole position is at $x_0 = -100\lambda$, $y_0 = 0\lambda$, for varying source/observation heights. Ground moisture is 10%, sea is saline water with a 32.5 *pp*/1000 salt content (see Table 1). Results for space wave (solid line) and total dipole fields (dashed line).

from the land/sea transition also decay at this rate, it is expected that the land/sea interface will have a significant effect on the total dipole fields and as is seen in these figures, the effect of the land/sea transition on the total fields is significant even at distances far from the transition. This is a very important and counter-intuitive result which has not been reported previously. A comment on the abrupt discontinuity observed at the reflection boundaries ($x = 100\lambda$) in all graphs seen in Figure 4. This discontinuity occurs where the reflected (GO) fields transition from those reflected from the ground to those reflected from the sea. Normally it would be expected that the addition of the diffracted fields to the total fields should produce uniform results across the reflection boundary, i.e., a smooth transition between the fields reflected from land and those reflected from water. The abrupt transition observed in these results can be explained by observing the impedance transition func-

tion for the seashore and its Fourier transform given in equations (20) and (21), respectively.

[32] In the perturbation formulation, the diffracted far field is proportional to the Fourier transform of the impedance transition function and therefore the discontinuity at the reflection boundaries observed in Figure 4 is a result of the phase reversal in equation (21) at $\alpha = 0$. Application of stationary phase techniques to obtain the far-field expression in equation (10) is in fact a sifting out of the dominant spectral component of the incident dipole fields (each spectral component corresponds to a plane wave). The discontinuity in equation (21) is caused by approximating the dipole fields incident on the transition as a single plane wave. A plane wave contains infinite energy across the impedance sheet, and by application of conservation of energy, the diffracted fields in the Fourier domain also contain infinite energy, which is contained in the impedance transition function at a point corresponding to the reflection boundary (noncontributing pole in the asymptotic analysis). This causes the nonphysical discontinuity seen at the reflection boundary in the results in Figure 4. To confirm this hypothesis, the transition function in the spatial domain (given in equation (20)) is weighted with a damping factor, or

$$h(x) = -sgn(x)e^{-\gamma|x|} \tag{25}$$

whose Fourier transform is given by

$$\tilde{h}(\alpha) = \frac{i\alpha}{\alpha^2 + \gamma^2}. \tag{26}$$

and which now contains finite energy. The diffracted fields produced by this transition function are compared to those from the original impedance transition function, with source and observation heights of 1λ (in Figure 4a). The results are shown in Figure 5. As expected, the effect of a damped transition, with finite energy smoothes the transition in the total fields across the reflection boundary (the field is continuous). While this result explains the apparent discontinuity in the fields across the reflection boundary it is not apparent as to how a to apply a damping factor which produces physical results. A more appropriate adjustment may be made to the direct dipole fields. While the plane wave approximation for the fields incident on the transition is a valid one, it does not account for the radiation pattern of the dipole and the decay of the dipole fields away from the transition. A proper solution however, can be obtained by considering an antenna with a radiation pattern whose spectral representation has a decay factor. In any case while the abrupt discontinuity across the reflection boundary is not in fact physical, the fields on either side of the boundary are correct.

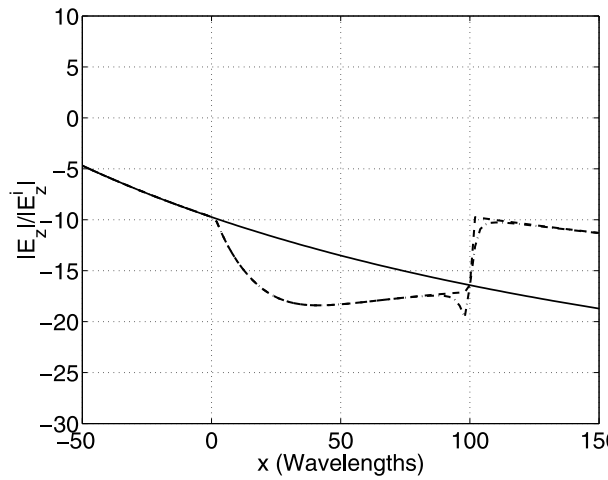

Figure 5. Magnitude (dB) of path loss at 30 MHz, for a land/sea transition, located at $x = 0$, z component of the electric fields for a vertical (z-directed) electric dipole. Transition width is 0λ (abrupt), observation $y = 0$, observation x from -50λ to 150λ. Dipole position is at $x_0 = -100\lambda$, $y_0 = 0\lambda$. Ground moisture is 10%, sea is saline water with a 32.5*pp*/1000 salt content (see Table 1). Results for space wave (solid line), total dipole fields, infinite transition function (dashed line), and total dipole fields, weighted transition function (dot-dashed line). See color version of this figure in the HTML.

[33] Finally in this section we show the effects of a land/sea transition on the total dipole fields as a function of frequency. We place an infinitesimal vertical electric dipole at $x_0 = -1000$ m, $y_0 = 0$ m (this is equivalent to placing the dipole at $x_0 = -100\lambda$, $y_0 = 0$ for the 30 MHz case, as in the previous examples). Figure 6 shows a comparison of the total dipole fields for operating frequencies of 30, 150, and 1000 MHz. For these results source and observation were held constant at 1λ above the impedance surface at each frequency. The observation point, as before, is on a straight line parallel to the surface, between source and observation and extends from $x = -500$ m to $x = 1500$ m. The impedance of the ground is again representative of San Antonio gray loam, with 10% gravimetric moisture content. As can be seen in Figure 6, while the overall field levels drop significantly, as frequency increases, the effect of the impedance transition (the trough in the graphs) does not change significantly, and in fact the range of its significance is maintained over frequency. The drop in overall field levels as a function of frequency can be explained by observing the GO reflection coefficient for an impedance surface, given by

$$\Gamma_v = \frac{\cos\theta_0 - \eta}{\cos\theta_0 + \eta}, \tag{27}$$

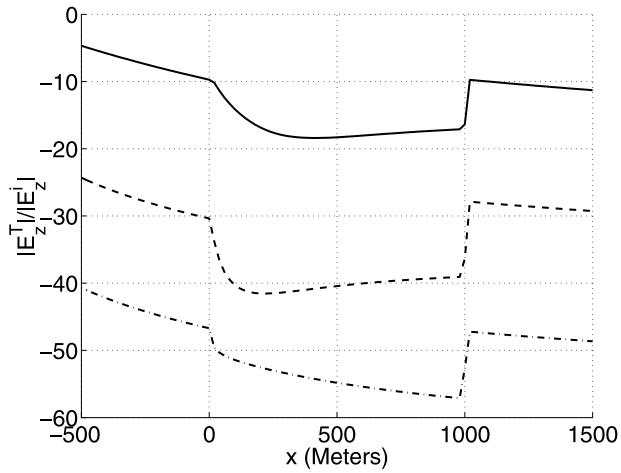

Figure 6. Total fields, magnitude (dB) of path loss at 30 MHz (solid line), 150 MHz (dashed line), and 1000 MHz (dot-dashed line) for a land/sea transition located at $x = 0$. Graph shows z components of the electric fields for a vertical (z-directed) electric dipole. Transition width is 0 m (abrupt), observation is at y = 0 m, with x varying from −500 m to 1500 m. Dipole position is at $x_0 = -1000$ m, $y_0 = 0$ m, with both source and observation 1λ above the impedance surface. Ground moisture is 10%, sea is saline water with a 32.5 *pp*/1000 salt content (see Table 1). See color version of this figure in the HTML.

where Γ_v is the vertical reflection coefficient, θ_0 is as the incident angle at the specular point. and η is the normalized surface impedance (mean impedance for the perturbation solution). Referring to equation (27), for the examples shown θ_0 is approaching $\pi/2$ (grazing incidence). At near grazing incidence the reflection coefficient is dominated by the normalized surface impedance. As the magnitude of the surface impedance increases, as a function of frequency (see values of normalized impedance given in Table 1) $\Gamma_v \rightarrow -1$, and thus the cancellation of the reflected field with the direct field increases.

3. Scattering and Diffraction in Presence of a Coastline

[34] In this section we will extend the model for shoreline diffraction to include the effects on the propagating radio wave of a cliff or bluff in proximity to the seashore. The effects of the cliff are modeled using standard 2-D GTD techniques for a 90° impedance wedge, both faces having the same impedance, and for plane wave incidence. All results are for TE polarization, TE being transverse electric, or electric field perpendicular to the 2-D plane of incidence (perpendicular to the plane of this paper). This extension of the model will account for the multiple interaction between the land/sea interface and the cliff, caused by incident radiation from secondary sources. In addition to reflection (GO fields) and diffraction effects from the primary incident fields, there are also secondary fields generated by 1) reflection and diffraction from the cliff face and edge, which acts as a secondary source exciting additional reflection and diffraction from the land/sea interface, and 2) reflection from the land/sea surface and diffraction from the land/sea transition which act as secondary sources exciting second-order reflection and diffraction from the cliff. Figure 7 shows the geometry of the coastline. The top view of Figure 7 shows the observation path for the results, with the middle and bottom views showing the various reflection and shadow boundaries in the GTD solution. Two sets of results will be included in this section, one for incidence excitation originating from the sea, and one for incidence excitation originating from the land, both at an angle of 30° from nadir (from vertical, see Figure 7). The fields included in the calculations for land and sea excitation are as follows.

3.1. Fields Included for Land Excitation

[35] First-order effects include a) reflection from the land/sea surface due to the direct field, b) reflection from the cliff top, due to the direct field, c) diffraction from the land/sea surface due to the direct field, and d) diffraction from the cliff edge due to the direct field.

[36] Second-order effects include e) reflection from the land/sea surface due to diffraction from the cliff edge, f) diffraction from the land/sea transition due to diffraction from the cliff edge, and g) diffraction from the cliff edge due to diffraction from the land/sea transition.

3.2. Fields Included for Sea Excitation

[37] First-order effects include a) reflection from the land/sea surface due to the direct field, b) reflection from the cliff face and top, due to the direct field, c) diffraction from the land/sea surface due to the direct field, and d) diffraction from the cliff edge due to the direct field.

[38] Second-order effects include e) reflection from the land/sea surface due to diffraction from the cliff edge, f) reflection from the land/sea surface due to reflection from the cliff face, g) reflection from the cliff face due to reflection from the land/sea surface, h) diffraction from the land/sea transition due to diffraction from the cliff edge, i) diffraction from the cliff edge due to reflection from the land/sea surface, and j) diffraction from the cliff edge due to diffraction from the land/sea transition.

3.3. Parameters Common to All Results

[39] For all results shown in this section, for excitation from both land and sea, and at all frequencies shown, the

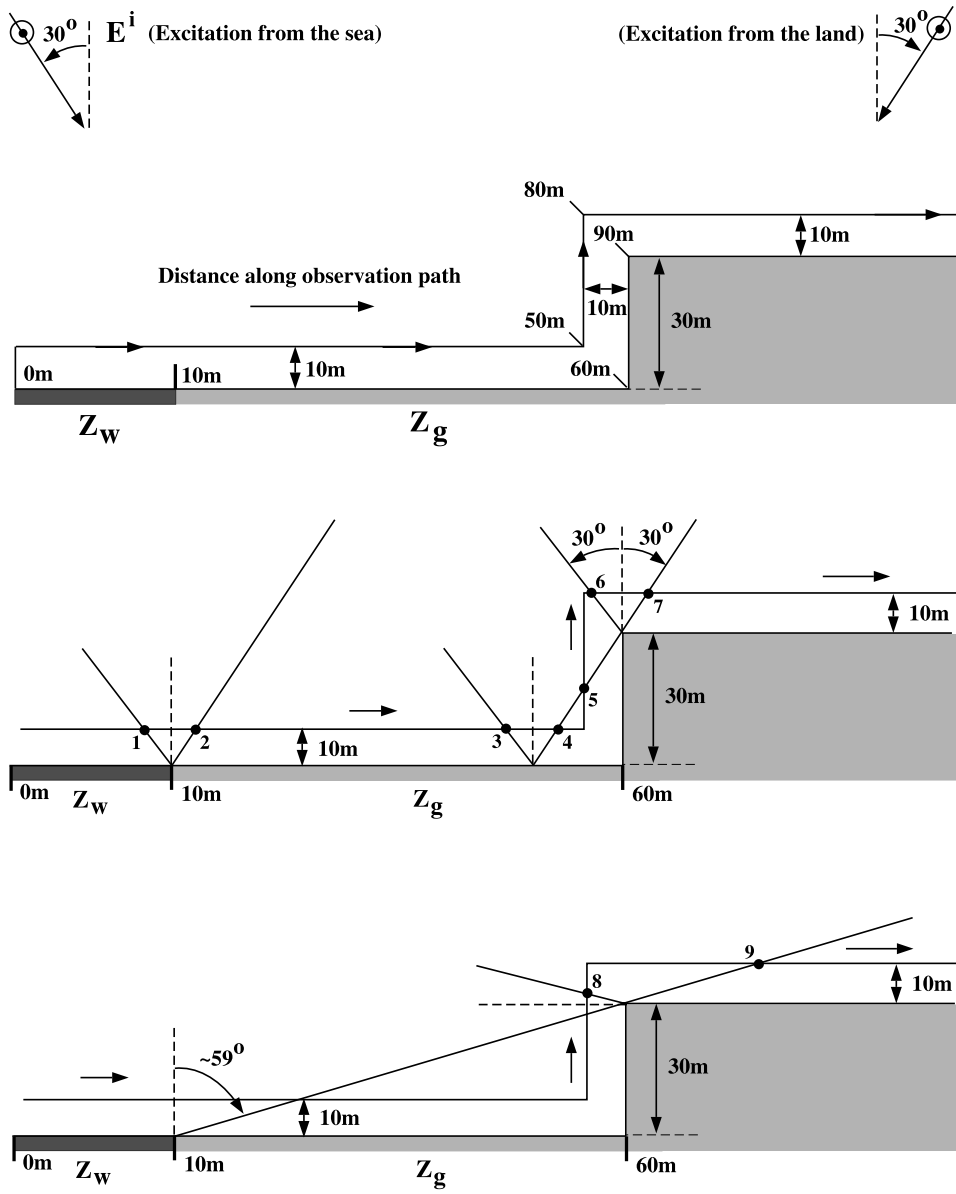

Figure 7. Cliff geometry showing reflection and shadow boundaries. See color version of this figure in the HTML.

ground is the same San Antonio gray loam as before, this time with a 20% gravimetric moisture content (again, refer to Table 1). In all graphs, the observation position (perhaps a UAV or helicopter) begins over the sea, at a 10 m height, comes in to within 10 m of the cliff face, rises vertically to a position 10 m above the top of the cliff, and then proceeds over the land above the cliff, also at a height of 10 m. This observation path is seen in the top view of Figure 7 and corresponds to the horizontal axis in the plotted results, while the vertical axis shown corresponds to path loss, as previously defined. Along this path 10 m corresponds to the position of the land/sea transition, with the area from 50 to 80 m, shown by the vertical bars in the graphs that follow, indicating the region where the observation platform is transitioning vertically, 10 m distance from the cliff face. The shoreline is 50 m away from the vertical cliff wall.

3.4. Results for Excitation From Land

[40] Results are shown for excitation from land in Figures 8, 9, and 10 for 30, 150, and 1000 MHz, respectively. Panels a in these plots show the total

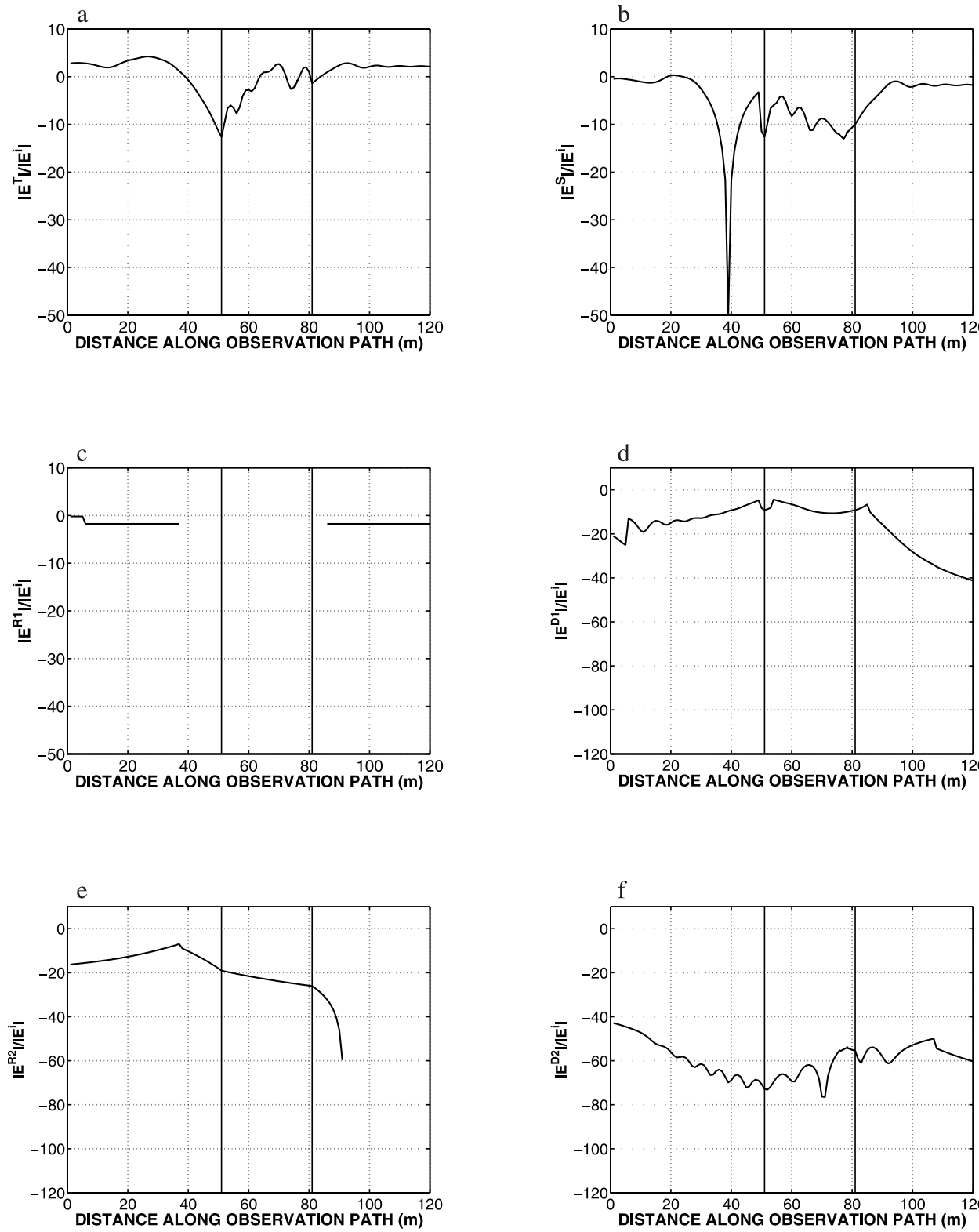

Figure 8. Scattering and diffraction from a coastline, 30 MHz, excitation from land.

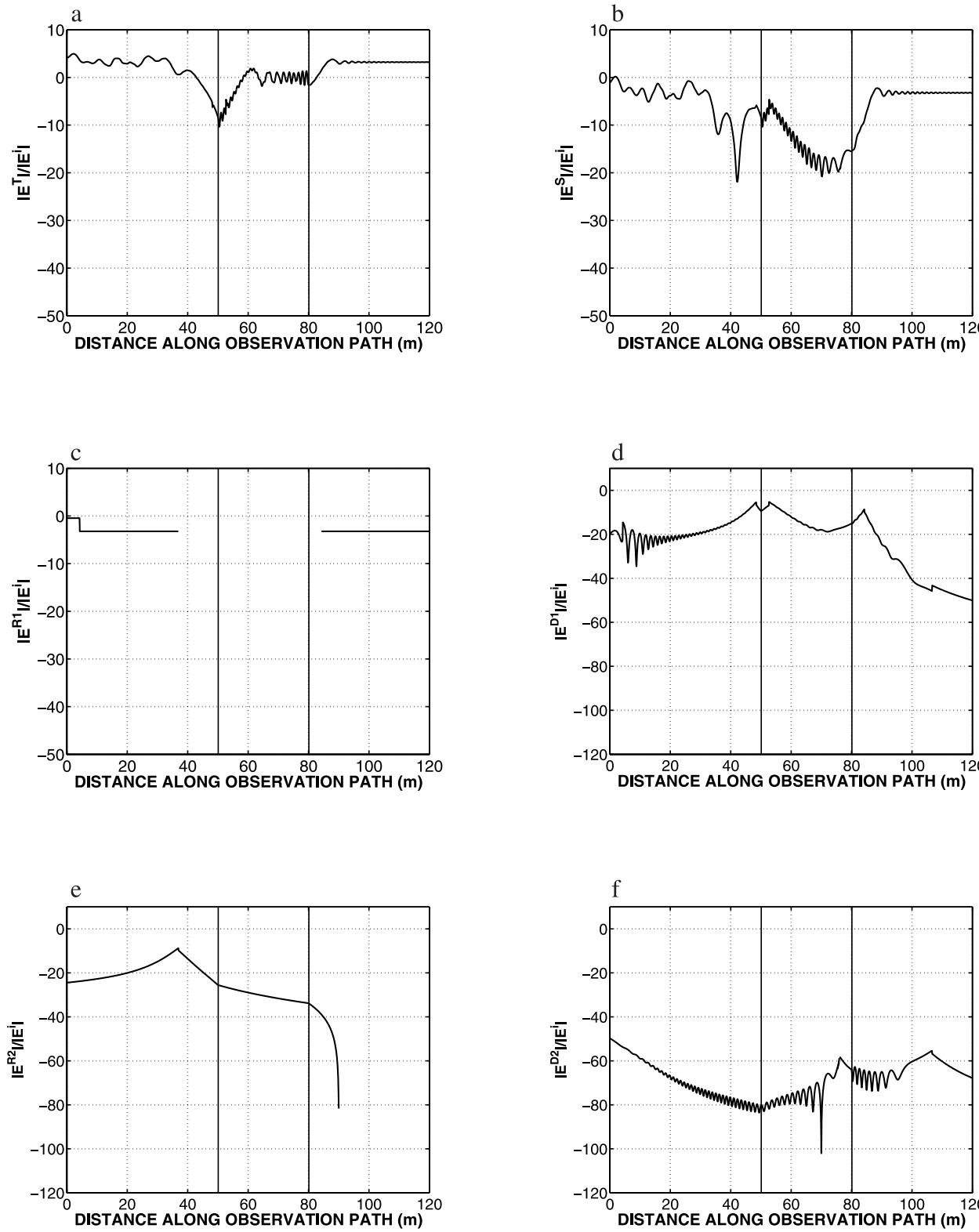

Figure 9. Scattering and diffraction from a coastline, 150 MHz, excitation from land.

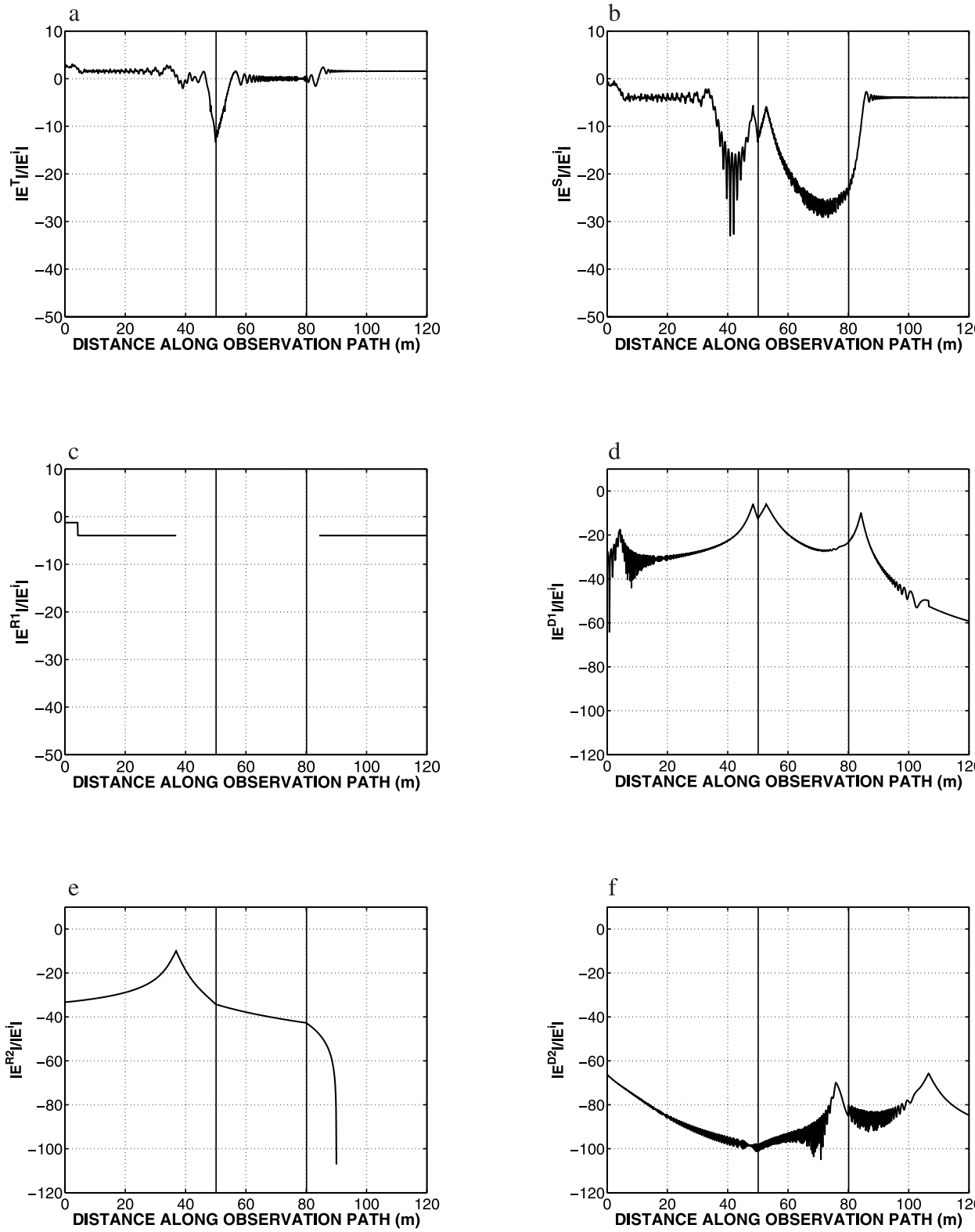

Figure 10. Scattering and diffraction from a coastline, 1000 MHz, excitation from land.

electric fields at the observation position, and panels b show the scattered fields (all fields except the direct). Panels c show the combined first-order reflected fields and include fields a and b in Section 3.1 above. Panels d in the land excitation plots show the combined first-order diffracted fields, and include fields c and d in Section 3.1. Panels e show the combined second-order reflected fields which are field e in Section 3.1. Panels f show the combined second-order diffracted fields, and include fields f and g in Section 3.1. Note that the scattered fields shown in panels b consist of the coherent sum of plots c–f.

[41] It is appropriate at this point to explain the various scattering and diffraction mechanisms observed in these plots. Referring to the first-order reflected fields, in Figures 8c, 9c, and 10c, the discontinuity at approximately 4.2 m observed in all of these plots is the reflection boundary caused by the land/sea transition, seen as point 1 in the center view of Figure 7. For observation positions less than 4.2 m the fields are those reflected from the sea, while at positions greater than 4.2 m the fields are those reflected from land. The absence of reflected fields between approximately 36.9 and 84 m is caused by reflection boundaries on the land/sea surface, and on the cliff edge, respectively, shown as points 3 and 6 in the center view of Figure 7. It is observed in these plots that as frequency is increased the reflected field levels decrease, and therefore do not have as significant an effect on the total field levels. This decrease in reflected field levels can be explained by observing the GO reflection coefficient for horizontal polarization given in equation (28) and the normalized impedances for 20% soil moisture shown in Table 1.

$$\Gamma_h = \frac{\eta \cos\theta_0 - 1}{\eta \cos\theta_0 + 1}. \tag{28}$$

As frequency is increased, the magnitude of the normalized impedance increases, and thus the magnitude of the horizontal reflection coefficient, Γ_h, becomes smaller. In Figures 8d, 9d, and 10d the first-order diffracted fields are observed. Noting that the discontinuities in diffracted fields are to compensate for shadow and reflection boundaries in the excitation fields, the first two discontinuities observed at approximately 48.5 and 52.7 m are caused by the observation position passing into and out of the shadow caused by the cliff edge on the direct field (see points 4 and 5 in the center view of Figure 7). The third discontinuity in these plots, at approximately 84.2 m, is the result of the reflection boundary caused by the cliff edge, as previously observed in plots c for the land excitation fields (point 6 in Figure 7). In Figures 8e, 9e, and 10e the second-order reflected fields are observed. There is one discontinuity at approximately 36.9 m, which corresponds to point 3 in Figure 7. This is caused by the diffracted ray from the cliff edge, which passes through the shadow boundaries at 48.5 and 52.7 m (points 4 and 5 in Figure 7), and is then reflected from the land/sea surface. Figures 8f, 9f, and 10f show the second-order diffracted fields. There are two additional discontinuities observed at approximately 76 and 106.7 m (the first is more obvious at higher frequencies). The first at 76 m, corresponding to point 8 in the bottom view of Figure 7, is caused by the reflection boundary at the cliff edge, when excited by the first-order diffraction from the land/sea interface. The second, shown as point 9 in the bottom view of Figure 7, is to compensate for the shadow boundary caused by the cliff edge on the excitation ray coming from the first-order diffracted ray caused by the land/sea interface.

[42] Of note in these plots is that the first-order reflected field (where it exists), as well as the first-order diffracted fields and second-order reflected fields in the neighborhood of all shadow and reflection boundaries, are of comparable magnitude, and their interaction will have a significant effect on the scattered field. The second-order diffracted fields, however, are of significantly lower levels throughout and therefore will not have an appreciable effect on the total scattered fields. This is observed in the total scattered fields in Figures 8b, 9b, and 10b. Of note in these plots is the region between approximately 30 and 90 m. In this area the first-order reflected fields do not exist, and there is significant interaction between the first-order diffracted fields and the second-order reflected fields. This effect is more prominent at 30 MHz, creating a significant fade at just below 40 m. At the higher frequencies of 150 and 1000 MHz the effects of these fields decrease, and the direct and first-order reflected fields dominate the total electric fields, as is seen in Figures 8a, 9a, and 10a.

3.5. Results for Excitation From the Sea

[43] Results are shown for excitation from sea in Figures 11, 12, and 13 for 30, 150, and 1000 MHz, respectively. Panels a in these plots show the total electric fields at the receiver position, and panels b show the scattered fields (all fields except the direct). Panels c show the combined first-order reflected fields and include fields a and b in Section 3.2. Panels d in the sea excitation plots show the combined first-order diffracted fields, and include fields c and d in Section 3.2. Panels e show the combined second-order reflected fields and include fields e–g in Section 3.2. Panels f in the same sea excitation plots show the combined second-order diffracted fields which consist of fields h–j in Section 3.2. Again the scattered fields shown in plot b consist of the coherent sum of the fields shown in plots c–f.

[44] The various scattering and diffraction mechanisms for excitation from the sea, seen in Figures 11, 12, and

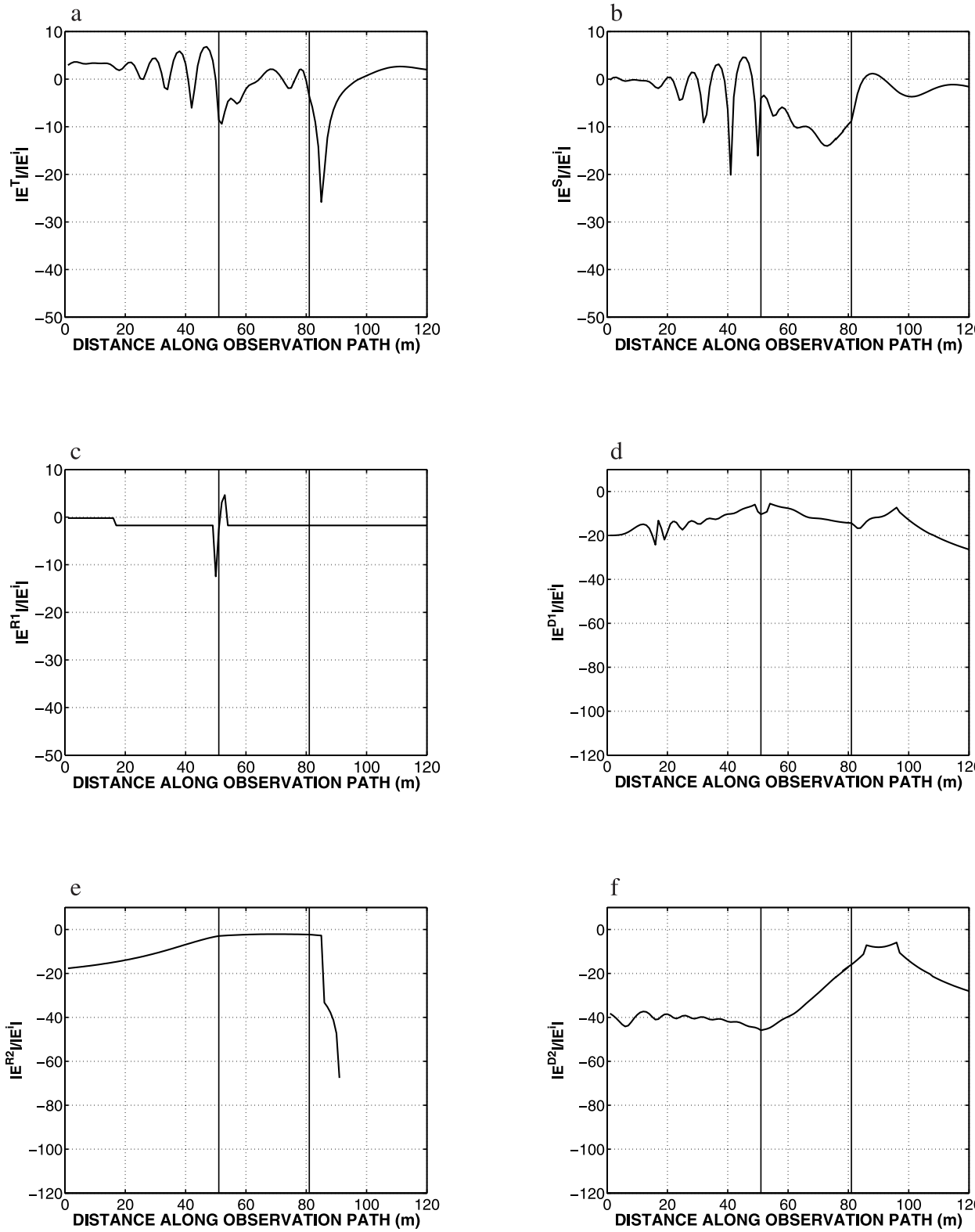

Figure 11. Scattering and diffraction from a coastline, 30 MHz, excitation from sea.

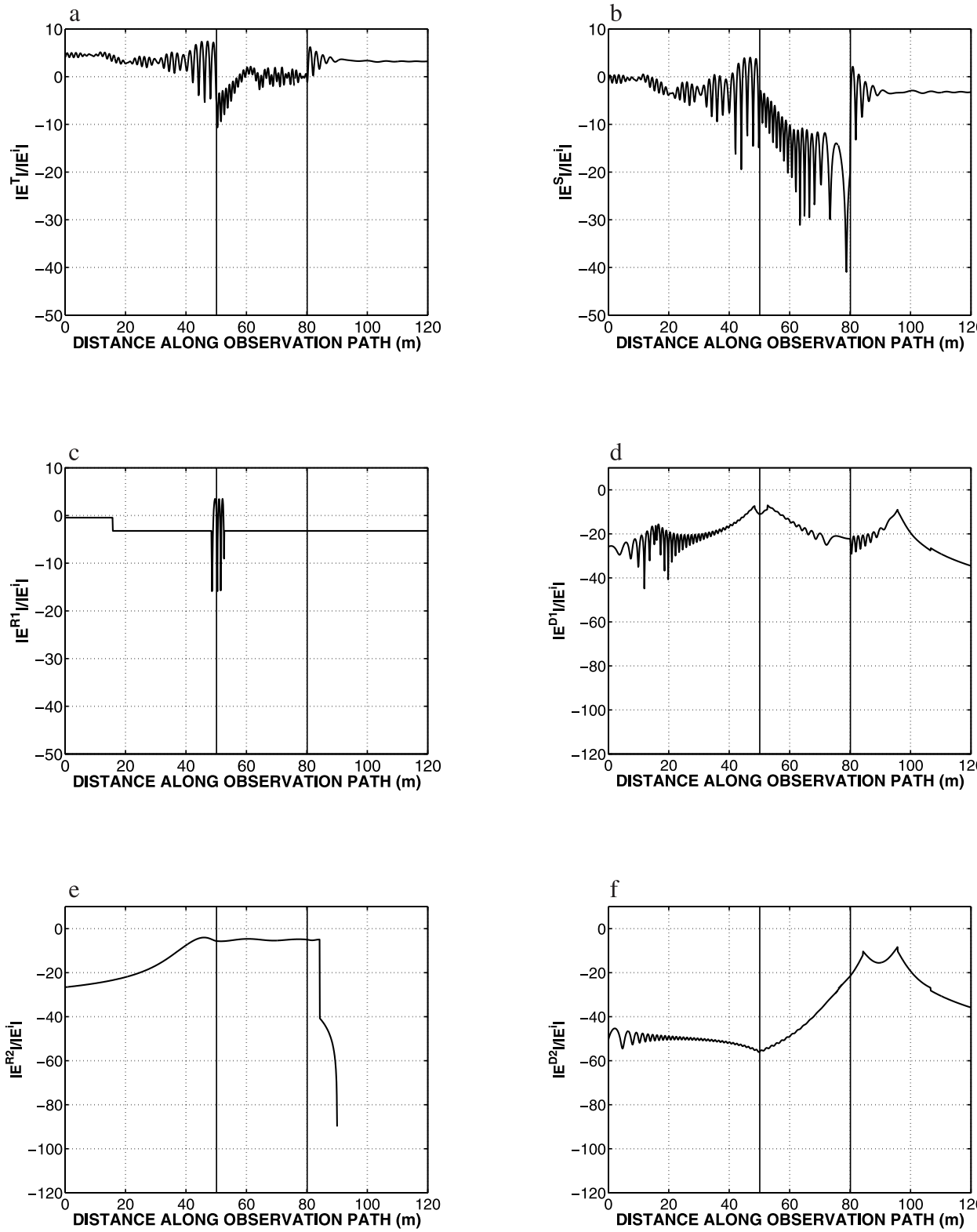

Figure 12. Scattering and diffraction from a coastline, 150 MHz, excitation from sea.

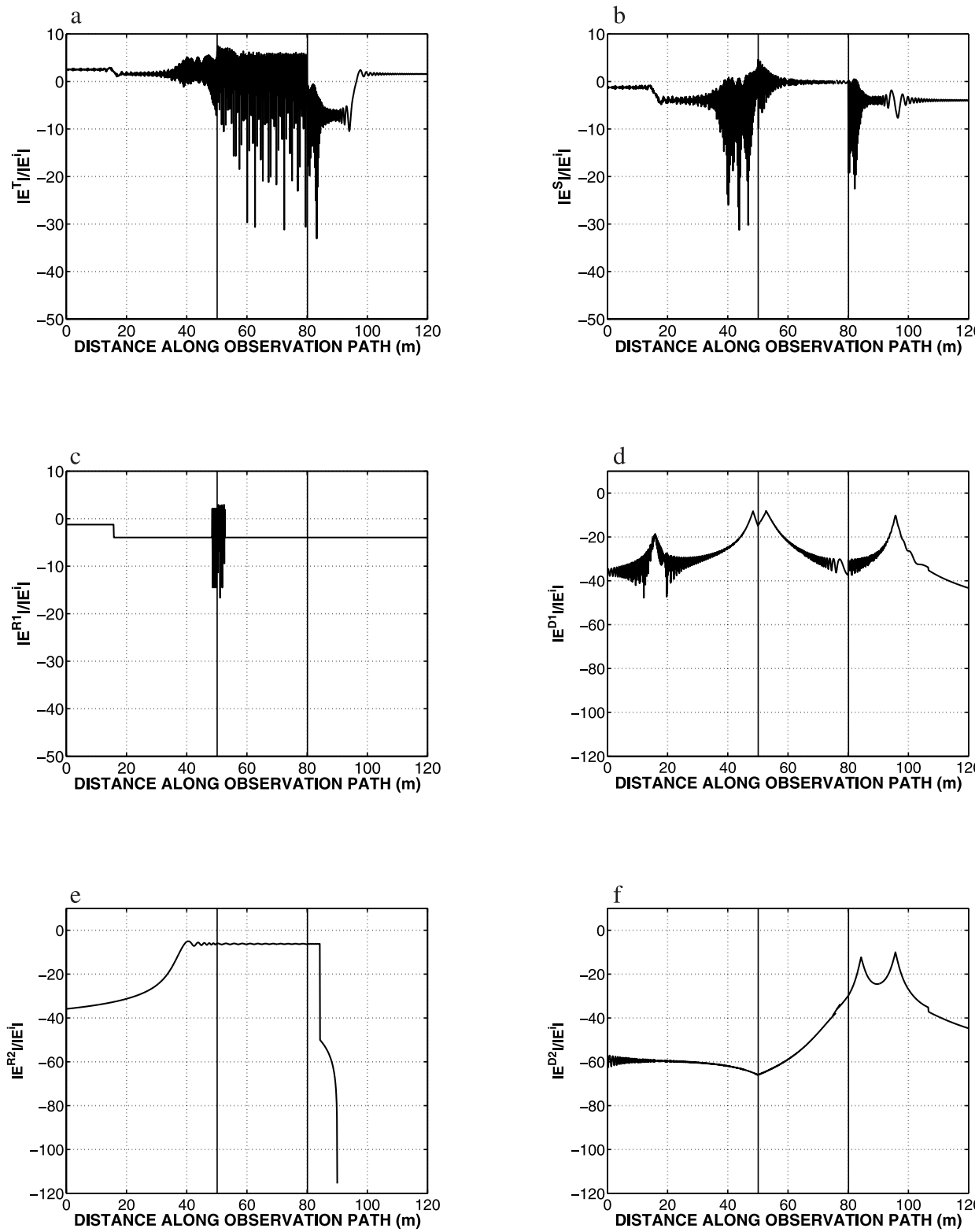

Figure 13. Scattering and diffraction from a coastline, 1000 MHz, excitation from sea.

13, are as follows. Referring to the first-order reflected fields, in Figures 11c, 12c, and 13c, the discontinuity at approximately 15.8 m observed in all of these plots is the reflection boundary caused by the land/sea transition, shown as point 2, in the center view of Figure 7. For observation position less than 15.8 m, the fields are those reflected from the sea, while at positions greater than 15.8 m the fields are those reflected from land. The level difference as a function of frequency for the fields reflected from the land are due to the same effects explained in the previous section, for excitation from the land. The oscillations which occur between approximately 48.5 and 52.7 m (points 4 and 5 in the center view of Figure 7), and at all frequencies, are caused by the interference between the first-order reflected wave from the sea, and that from the cliff face. As both fields are of a comparable level, the level of these oscillations is significant. In Figures 11d, 12d, and 13d the first-order diffracted fields are observed. Again, remembering that the discontinuities in diffracted fields are to compensate for shadow and reflection boundaries in the excitation fields, the first two discontinuities observed at approximately 48.5 and 52.7 m (points 4 and 5 in Figure 7) represent the boundaries, within which the first-order field reflected by the cliff face exists. This corresponds to the regions of oscillation in the first-order reflected fields discussed earlier. The third discontinuity at approximately 95.8 m is from the reflection boundary caused by the direct field incident on the cliff edge, seen as point 7 in Figure 7. In Figures 11e, 12e, and 13e the second-order reflected fields for sea excitation are observed. From 0 to approximately 36.9 m (point 3 in Figure 7) and beyond approximately 84.2 m (point 6 in the same figure), the second-order reflected fields consist of reflections from the land/sea surface caused by the first-order cliff diffraction. In the region between 36.9 and 84.2 m the second-order reflected fields observed are dominated by the double bounce reflection between the cliff face and the land/sea surface, and vice versa. Note the significant fields levels in this region. Figures 11f, 12f, and 13f show the second-order diffracted fields. There are two discontinuities observed at approximately 84.2 and 95.8 m (points 6 and 7 in Figure 7). These are caused by the reflection boundary of the second-order excitation of the cliff edge by the ray reflected from the land/sea surface, and the shadow boundary of the same ray, respectively. Note that there are two additional discontinuities in the second-order diffracted fields, at 76 and 106.7 m caused by the reflection and shadow boundaries of second-order excitation of the cliff edge by the land/sea interface, shown as points 8 and 9 in the bottom view of Figure 7. These fields, however, are of a level significantly lower than the other second-order diffracted fields, and therefore are not obvious in the plots.

[45] Of note in these plots is that all first- and second-order field components, both reflected and diffracted, contain field levels of comparable magnitude, and therefore all will have a significant effect on the total scattered fields. This can be seen in the total scattered fields in Figures 11b, 12b, and 13b. Of note in these plots is the significant interference pattern, with significant fades, in the region between approximately 20 and 90 m. In this region the second-order reflected fields begin to interfere appreciable with the other fields. As before, these effects are more prominent at 30 MHz and at the higher frequencies tend to decrease. The total fields, seen in Figures 8a, 9a, and 10a, show a similar pattern, as the scattered fields interfere with the direct.

4. Summary

[46] The effects on the total fields of an infinitesimal electric dipole by a land/sea transition were first examined by application of a perturbation technique. The land/sea transition is modeled as a perturbation in a surrounding homogeneous impedance. Noting that the $\hat{z}$ component of the received electric fields from a vertical dipole are dominant for source and observation near the impedance surface, this case was analyzed. In order to apply the perturbation technique in the Fourier domain the impedance transition function was dealt with in a mean sense, which is an acceptable approximation for source and observation near the impedance surface. When either source or observation are raised above the surface, the assumption of a mean impedance is no longer valid, however, for this scenario the diffracted fields are minimal and the space wave (direct + GO) dominate the received fields.

[47] The effect of the gradient of the impedance transition from land to sea was first analyzed. It was shown that while a more gradual transition tends to focus the scattered field energy in the specular direction, the field levels in the neighborhood around specular scattering were essentially unaffected, thus indicating that for source and observation near the impedance surface, where the observation position always tends to be in the specular direction, the effects of the transition width can be ignored. Observation of the path loss of the total fields when compared with that of the space wave (direct + GO) showed that the land/sea transition has a significant effect on the total dipole fields, even distant from the seashore, again for the case of source and observation near the surface.

[48] In addition, the effects of a cliff or shoreline in close proximity to the seashore was examined. Scattered and total fields for excitation originating from both land and sea, showed significant effects from reflected and diffracted fields, especially from the region near and in the vertical transition of the observation platform along

the cliff face. For both excitations fades were more significant at lower frequencies, as the reflected fields tended to be at a higher level for these frequencies. A significant oscillatory behavior was observed when the excitation originated from the sea. For excitation from land, it was observed that the second-order diffracted fields were to low to appreciably effect the scattered and total fields.

[49] **Acknowledgments.** The authors gratefully acknowledge the support of the National Science Foundation under contract ECS-9979376 and the DARPA FCS Communications project under subcontract S01-19 from the Pennsylvania State University.

References

Bazer, J., and S. N. Karp, Propagation of plane electromagnetic waves past a shoreline, *J. Res. Natl. Bur. Stand., Sect. D*, *66*, 319–334, 1962.

Boersma, J., and Y. Rahmat-Samii, Comparison of two leading uniform theories of edge diffraction with the exact uniform asymptotic solution, *Radio Sci.*, *15*, 1179–1194, 1980.

Clemmow, P. C., Some extensions to the method of integration by steepest descents, *Q. J. Mech. Appl. Math., Part 2*, *3*, 241–256, 1950.

Clemmow, P. C., Radio wave propagation over a flat Earth across a boundary separating two different media, *Philos. Trans. R. Soc. London, Ser. A*, *246*, 1–55, 1953.

de Jong, G., Electromagnetic wave propagation over an inhomogeneous flat Earth (two-dimensional integral equation formulation), *Radio Sci.*, *10*, 925–933, 1975.

Felsen, L. B., and N. Marcuvitz, *Radiation and Scattering of Waves*, IEEE Press, Piscataway, N. J., 1994.

Hipp, J. E., Soil electromagnetic parameters as functions of frequency, soil density, and soil moisture, *Proc. IEEE*, *62*, 98–103, 1974.

Maliuzhinets, G. D., Excitation, reflection, and emission of surface waves from a wedge with given face impedances, *Sov. Phys. Dokl.*, *3*, 752–755, 1958.

Norton, K. A., Propagation of radio waves over the surface of the Earth and in the upper atmosphere: Part I, *Proc. IRE*, *24*, 1367–1387, 1936.

Norton, K. A., Propagation of radio waves over the surface of the Earth and in the upper atmosphere: Part II, *Proc. IRE*, *25*, 1203–1236, 1937.

Ott, R. H., RING: An integral equation algorithm for HF-VHF radio wave propagation over irregular, inhomogeneous terrain, *Radio Sci.*, *27*, 867–882, 1992.

Sarabandi, K., Scattering from variable resistive and impedance sheets, *J. Electromagn. Waves Appl.*, *4*, 865–891, 1990.

Sarabandi, K., and M. D. Casciato, Diffraction of radio waves from arbitrary one-dimensional surface impedance discontinuities, *IEEE Trans. Antennas Propag.*, *47*, 86–96, 1999.

Sarabandi, K., M. D. Casciato, and I. Koh, Efficient calculation of the fields of a dipole radiating above an impedance surface, *IEEE Trans. Antennas Propag.*, *50*, 1222–1235, 2002.

Senior, T. B. A., and J. L. Volakis, *Approximate Boundary Conditions in Electromagnetics*, IEE Press, London, UK, 1995.

Sklar, B., *Digital Communications, Fundamentals and Applications*, Prentice-Hall, Old Tappan, N. J., 1988.

Ulaby, F. T., R. K. Moore, and A. K. Fung, *Microwave Remote Sensing, Active and Passive*, vols. 1, 2, and 3, Artech House, Norwood, Mass., 1986.

Wait, J. R., Recent analytical investigations of electromagnetic ground wave propagation over inhomogeneous Earth models, *Proc. IEEE*, *62*, 1061–1072, 1974.

M. D. Casciato, S. Oveisgharan, and K. Sarabandi, Radiation Laboratory, Department of Electrical Engineering and Computer Science, University of Michigan, Ann Arbor, MI 48109-2122, USA. (casciato@eecs.umich.edu; saraband@eecs.umich.edu)